

D3

N79-27078

TREATMENT OF THE CONTROL MECHANISMS OF LIGHT AIRPLANES  
IN THE FLUTTER CLEARANCE PROCESS

Elmar J. Breitbach\*  
Langley Research Center

SUMMARY

Recently, it has become more and more evident that many difficulties encountered in the course of aircraft flutter analyses can be traced to strong localized nonlinearities in the control mechanisms. To cope with these problems, more reliable mathematical models paying special attention to control system nonlinearities may be established by means of modified ground vibration test procedures in combination with suitably adapted modal synthesis approaches. Three different concepts are presented in detail.

INTRODUCTION

At first glance the flutter clearance of soaring and light airplanes does not seem to raise any serious problems which cannot be solved by means of today's aeroelastic tools. This is true even for the determination of the unsteady aerodynamic loads as long as cases with large aspect ratios at comparably low speeds are considered. The elastodynamical characteristics can be determined by using common experimental or analytical methods if structural linearity can be assumed to be a proper approximation. However, as experience has shown, the control mechanisms of light airplanes<sup>1</sup> are generally nonlinear to such a large extent that setting up a dependable mathematical model requires special attention, including modifications to standard linearized procedures.

In the first part of this paper some of the most frequently occurring types of control-system nonlinearities are described. To get an idea of the influence of some typical nonlinearities on the aeroelastic stability the results of wind tunnel flutter tests on a nonlinear wing aileron model are presented. After that, it is shown in detail how the aeroelastic equations of light airplanes with localized nonlinearities may be formulated by using various suitably modified ground vibration test (GVT) procedures all based on the well-known modal synthesis approach. The shortcomings as well as the usefulness of the different concepts are discussed.

---

\*NRC-NASA Senior Resident Research Associate.

<sup>1</sup>Light airplanes as used in this paper include both powered and unpowered vehicles where the power to the flight control system is supplied by the pilot without electrical or hydraulic boost through a system of cables, pulleys, push-rods, bellcranks, or other mechanical linkages.

## SYMBOLS

a,b	hinge axis coordinates of control surfaces and tabs, respectively
A,B,C	mass, damping, and stiffness matrices, respectively, defined in terms of geometrical displacements
$\Delta A, \Delta B, \Delta C$	matrices of mass, damping, and stiffness changes, respectively, defined in terms of geometrical displacements
$C_e$	equivalent linear stiffness of a nonlinear force deflection diagram, defined in equations (1) and (2)
e,f	center-of-gravity coordinates of control surfaces and tabs, respectively
F	force or moment acting on a control surface or tab
g	column matrix of constraint functions $g_{\ell}$
h	bending deflection of the quarter-chord line of lifting surface
$I_v, I_{tv}$	mass moments of inertia per span unit of control surface and tab, respectively, referred to the center of gravity
$I_{Rx}, I_{Ry}, I_{Rz}$	mass moments of inertia of control surface referred to the main axes of inertia
$\ell$	span width coordinate
$m_R$	control-surface mass
$m_v, m_{tv}$	mass per unit span of control surface and tab, respectively
M,D,K	generalized mass, damping, and stiffness matrices, respectively
$\Delta M, \Delta D, \Delta K$	generalized matrices taking into account mass, damping, and stiffness changes, respectively
P	column matrix of external forces
q,P	column matrices of generalized coordinates
Q	column matrix of generalized forces
t	time
T	inertia energy
u	column matrix of geometrical deflections
U	stiffness energy

v flight speed  
 W damping energy  
 X,Y transformation matrices, defined in equations (53) and (55)  
 $\alpha$  rotation about the quarter-chord line of lifting surface  
 $\beta$  control-surface rotation about the hinge line  
 $\gamma$  tab rotation about tab hinge line  
 $\eta$  rotation of a control surface referred to its center of gravity  
 $\theta$  damping loss angle  
 $\lambda$  column matrix of Lagrange's multipliers  $\lambda_l$   
 $\Lambda$  diagonal matrix of the square values of the normal circular frequencies  
 $\Phi, \Psi$  modal matrices  
 $\omega$  circular frequency  
 I unity matrix  
 O zero matrix  
 $j = \sqrt{-1}$  imaginary unit

Subscripts:

A,B,C,R,v,t substructures indices  
 l constraint index,  $l = 1, 2, \dots, \sigma$   
 r normal mode index  
 $\sigma, \epsilon$  indices referring to  $\sigma$  constraints and  $\epsilon$  independent coordinates  
 NL index referring to nonlinear properties  
 L index referring to linear properties

Superscripts:

T transposed matrix  
 A,B indices referring to substructures A and B  
 ', " real, imaginary part

## GENERAL REMARKS

### Sources of Control-System Nonlinearities

Aeroelastic investigations are usually carried out on the basis of simplified linearized mathematical models. In many cases this approach has been adequate to ensure sufficient flutter safety margins for light airplanes. However, in the last few years, it has become evident that disregarding nonlinear phenomena can lead to hazardously misleading results. For example, it is shown in reference 1 that so-called concentrated or localized nonlinearities in control systems have a significant effect on the flutter behavior. Nonlinearities of this kind may be produced by such things as

- (1) Backlash in the joints and linkage elements
- (2) Solid friction in control-cable and pushrod ducts as well as in the hinge bearings
- (3) Kinematic limitation of the control-surface stroke
- (4) Application of special spring tab systems provided for pilot handling relief

The most critical parts of a control mechanism where localized nonlinearities may arise are shown schematically in figure 1.

An aeroelastic investigation may become even more complicated if it is necessary to account for items such as the following:

- (1) Preload changes due to maneuver loads and specially trimmed flight attitudes
- (2) Changes in friction and backlash over an airplane's lifetime
- (3) Additional mass, stiffness, and damping forces randomly activated by the pilot

Coping with all these difficulties requires special measures throughout the flutter clearance process. First, the ground vibration test (GVT) used to determine the elastodynamical coefficients of the flutter equations has to be modified so that a consistent and superpositionable set of orthogonal, or well-defined nonorthogonal, normal modes can be measured.

In reference 2 a proposed experimental approach employs a high frequency auxiliary excitation superimposed upon the much lower sinusoidal excitation to be tuned to the several normal frequencies. Thus, "slip-stick" effects and related nonlinearities in the control mechanisms can be minimized. The method requires additional test and control devices capable of exciting all controls simultaneously.

Of course, the simplest solution appears to be to build control-surface mechanisms without either friction or backlash. However, aside from a consider-

able increase in manufacturing costs, there is no guarantee that such an ideal condition could be kept unchanged for the lifetime of an airplane. Moreover, a frictionless control system is not necessarily equivalent to better handling qualities, because friction helps give the pilot the "feel" of flying the airplane.

From an experimentalist's standpoint, there are some simpler, but effective, methods using special modal coupling and modal superposition approaches. A detailed presentation of some of these methods is given in the subsequent sections of this paper. They will be referred to as Concepts I, II, and III.

#### Illustrative Examples of Control-System Nonlinearities

To get a realistic impression of control-mechanism nonlinearities, the force deflection diagrams  $F(\beta)$  of the rudder and aileron system (antisymmetrical and symmetrical case) of a soaring airplane (ASW-15, A. Schleicher, Poppenhausen, W. Germany) are shown in figures 2(a), 3(a), and 4(a). Using the principle of the energetic equivalence (refs. 1 and 3) the stiffness and damping properties of a nonlinear force deflection diagram can be approximated by the so-called equivalent complex stiffness:

$$C_e(\beta) = C_e'(\beta) + j C_e''(\beta) \quad (j = \sqrt{-1}) \quad (1)$$

The coefficients  $C_e'(\beta)$  and  $C_e''(\beta)$ , representing stiffness and damping, respectively, can be calculated from

$$\left. \begin{aligned} C_e'(\beta) &= \frac{1}{\pi\beta} \int_{\phi=0}^{2\pi} F(\beta \cos \phi, -\beta\omega \sin \phi) \cos \phi \, d\phi \\ C_e''(\beta) &= \frac{1}{\pi\beta} \int_{\phi=0}^{2\pi} F(\beta \cos \phi, -\beta\omega \sin \phi) \sin \phi \, d\phi \end{aligned} \right\} \quad (2)$$

where the circular frequency  $\omega = 2\pi f$  (where  $f$  is frequency in hertz) and the integration variable  $\phi = \omega t$ . Damping can also be expressed by the loss angle

$$\theta_e(\beta) = \frac{C_e''(\beta)}{C_e'(\beta)} \quad (3)$$

The functions  $C_e^i(\beta)$  and  $C_e^a(\beta)$  corresponding to the force deflection diagrams of figures 2(a), 3(a), and 4(a) are plotted in 2(b), 3(b), and 4(b), respectively. Figure 3(b) shows that the antisymmetric aileron hinge stiffness in the range of the normal aileron stroke varies between 390 N-m and 44 N-m. Because of the stiffness variation, the normal frequency of the antisymmetrical aileron vibration (wing assumed to be fixed) varies over a wide range, between 2.4 Hz and 7.4 Hz. At least two other antisymmetric normal modes lie in this frequency range and are consequently characterized by highly amplitude-dependent portions of aileron vibrations. Similar effects can also be observed for the symmetric aileron mode and for the rudder vibration.

The effects of strong nonlinearities on the flutter behavior have been demonstrated in some wind-tunnel tests carried out on a nonlinear wing-aileron model in the low-speed wind tunnel of DFVLR Göttingen. The nonlinear flutter boundaries for a backlash-type and for a spring-tab-type aileron hinge stiffness are shown in figure 5. Unlike the flutter boundaries of linear systems, both curves are characterized by a considerable dependence of the critical flutter speed on the aileron amplitude. Thus, the flutter boundary of the spring-tab-type system varies between  $V = 12.5$  m/s and  $V = 24$  m/s. The backlash-type system shows a flutter boundary variation between  $V = 13.5$  m/s and  $V = 20$  m/s. More detailed information, especially about the geometric and elastodynamic data of the wing-aileron model, is presented in reference 1.

#### MATHEMATICAL MODELING USING MODAL SYNTHESIS CONCEPTS

As mentioned previously, the determination of the elastodynamic characteristics by means of GVT can be affected severely by localized nonlinearities in the control mechanisms. It will be shown in the following discussion that the uncertainties resulting from these nonlinear effects can be avoided by applying experimental-analytical concepts based on the well-known modal synthesis approach.

Each of these concepts can be used to set up the aeroelastic equations of the actual airplane including all control-mechanism nonlinearities. The nonlinear force deflection diagrams of the different controls can be determined by static or dynamic tests.

Three different concepts will be presented. They may be briefly described as follows:

Concept I: Measurement of a set of orthogonal normal modes with the control surfaces rigidly clamped; separate determination of the control-surface normal modes with the rest of the airplane rigidly fixed.

Concept II: GVT on a configuration artificially linearized by replacing the nonlinear control-mechanism elements by linear and lightly damped dummy devices; thus, a set of orthogonal normal modes for the entire system is available.

Concept III: Measurement of a set of orthogonal normal modes with the control surfaces removed; separate determination of the normal modes of the control surfaces in uncoupled condition.

### Concept I

The governing equations of motion of an aeroelastic system, formulated in terms of physical coordinates, can be written in matrix notation as follows:

$$A\ddot{u} + B\dot{u} + Cu = P \quad (4)$$

where

- A mass matrix
- B damping matrix
- C stiffness matrix
- u column matrix of the physical displacements;  $\dot{u}$  and  $\ddot{u}$  are first and second derivatives with respect to time t
- P column matrix of external forces, for instance, unsteady aerodynamic forces

It is obvious that parts of the matrices B and C are nonlinear because of the localized nonlinearities of the controls.

Controls without tabs. - If the GVT is carried out with the controls rigidly clamped to the adjacent structure, a set of n largely linear normal modes  $\phi_{Ar}$  can be measured and combined in the modal matrix

$$\Phi_A = [\phi_{A1}, \phi_{A2}, \dots, \phi_{Ar}, \dots, \phi_{An}] \quad (5)$$

The modes satisfy the orthogonality condition

$$\left. \begin{aligned} \Phi_A^T A \Phi_A &= M_A \\ \Phi_A^T C \Phi_A &= \Lambda_A M_A = K_A \end{aligned} \right\} \quad (6)$$

where

- $M_A$  diagonal matrix of the generalized masses  $M_{Ar}$
- $K_A$  diagonal matrix of the generalized stiffnesses  $K_{Ar} = \omega_{Ar}^2 M_{Ar}$

$\Lambda_A$  diagonal matrix of the square values of the circular normal frequencies  $\omega_{Ar}$

The generalized damping matrix  $D_A$  (not necessarily diagonal) is defined by

$$D_A = \Phi_A^T B \Phi_A \quad (7)$$

Next, assuming that the control surfaces are rigid in the frequency range of interest, a number of additional control-surface rotation modes with the adjacent main structure at rest can be determined and combined in the modal matrix

$$\Phi_B = [\phi_{B1}, \phi_{B2}, \dots, \phi_{Bv}, \dots, \phi_{Bm}] \quad (8)$$

The physical displacements of the complete structure are related to the generalized coordinates by

$$u = \Phi q \quad (9)$$

where the column matrix of the generalized coordinates  $q_r$  and  $q_v$  is

$$q = [q_A^T, q_B^T]^T \quad (10)$$

and

$$\Phi = [\Phi_A, \Phi_B] \quad (11)$$

The basic idea of this modal superposition is outlined in figure 6. Substituting equation (9) into equation (4) and premultiplying it by  $\Phi^T$  yields

$$M\ddot{q} + D\dot{q} + Kq = Q \quad (12)$$

where

$$\left. \begin{aligned}
 M &= \begin{bmatrix} M_A & M_{AB} \\ M_{BA} & M_B \end{bmatrix} & Q &= \phi^T P \\
 D &= \begin{bmatrix} D_A & 0 \\ 0 & D_B \end{bmatrix} & K &= \begin{bmatrix} K_A & 0 \\ 0 & K_B \end{bmatrix}
 \end{aligned} \right\} \quad (13)$$

The matrices  $M_A$ ,  $K_A$ , and  $D_A$  measured in a GVT are defined in the equations (6) and (7). The diagonal matrices  $M_B$ ,  $D_B$ , and  $K_B$  contain the generalized masses, damping values, and stiffnesses of the control-surface rotation modes. In the case of nonlinear hinge stiffness and damping, the matrix elements of  $K_B$  and  $D_B$  are

$$K_{Bv} = C'_{ev}(\beta) \beta_{va}^2 \quad D_{Bv} = \frac{C''_{ev}(\beta)}{\omega} \beta_{va}^2 \quad (14)$$

where  $C'_{ev}(\beta)$  and  $C''_{ev}(\beta)$  can be determined from equation (2). The term  $\beta_{va}$  denotes the control rotation in the action line of the control actuator force. The matrix  $M_B$  can be determined by calculation or measurement taking into account not only the control-surface mass but also the moving mass of such attached hardware as pushrods, cables, and control stick. The elements of the coupling matrix

$$M_{AB} = M_{BA}^T = \phi_A^T A \phi_B \quad (15)$$

can be found by integration over surfaces  $S_{Bv}$  of the controls

$$M_{AB,rv} = \int_{S_{Bv}} \{ e_v m_v h_r \beta_v + [I_v + e_v m_v (a_v + e_v)] \alpha_r \beta_v \} d\ell \quad (16)$$

where the following terms correspond to the  $v$ th control with tab locked to the control

- $m_v$  mass of the control surface per unit span
- $I_v$  mass moment of inertia per unit span referred to the center of gravity
- $e_v$  distance between center of gravity and hinge axis (see fig. 7)
- $a_v$  distance between hinge axis and the quarter-chord point (see fig. 7)

All these data as well as the amplitudes  $h_r$ ,  $\alpha_r$ , and  $\beta_v$  (see fig. 7) are functions of the span coordinate  $\ell$ . In case of an ideal locking of the con-

trols, neither hinge stiffness forces nor hinge damping forces are generated in the normal modes  $\phi_{Ar}$ . Hence,

$$\left. \begin{aligned} K_{AB} &= K_{BA}^T \equiv 0 \\ D_{AB} &= D_{BA}^T \equiv 0 \end{aligned} \right\} \quad (17)$$

Extension to controls with tabs.— The above procedure can easily be extended to systems with controls and tabs (spring tabs, trim tabs, or geared tabs) by introducing the tab movement as a separate degree of freedom. For this special case the main GVT configuration is characterized by controls locked to the adjacent airplane structure and tabs locked to the controls. This leads to the same set of normal modes  $\phi_{Ar}$  as defined in equation (5). Furthermore, the degrees of freedom of the controls are separately determined with the main structure at rest and with tabs locked to the controls. The resulting normal modes are identical to the ones defined by equation (8). Finally, in a third step the tab modes  $\phi_{Cv}$  are determined with both the main structure and the controls at rest. This concept is schematically illustrated in figure 8. In accordance with this,  $u$  can be expressed as a series expansion of the normal mode sets  $\phi_A$ ,  $\phi_B$ , and  $\phi_C$

$$u = [\phi_A, \phi_B, \phi_C] q \quad (18)$$

where

$$q = [q_B^T, q_B^T, q_C^T]^T \quad (19)$$

Replacement of  $u$  in equation (4) by equation (18) and premultiplication by  $\phi^T$  leads to an equation similar to equation (12). Because of the additional tab degrees of freedom the matrices  $M$ ,  $D$ ,  $K$ , and  $Q$  have the extended form

$$\left. \begin{aligned} M &= \begin{bmatrix} M_A & M_{AB} & M_{AC} \\ M_{BA} & M_B & M_{BC} \\ M_{CA} & M_{CB} & M_C \end{bmatrix} & Q &= \phi^T p \\ D &= \begin{bmatrix} D_A & 0 & 0 \\ 0 & D_B & 0 \\ 0 & 0 & D_C \end{bmatrix} & K &= \begin{bmatrix} K_A & 0 & 0 \\ 0 & K_B & 0 \\ 0 & 0 & K_C \end{bmatrix} \end{aligned} \right\} \quad (20)$$

The matrices  $M_A$ ,  $M_B$ ,  $M_{AB} = M_{BA}^T$ ,  $K_A$ ,  $K_B$ ,  $D_A$ , and  $D_B$  are identical to the matrices defined in equations (6), (7), (14), (15), and (16). The matrices  $K_C$  and  $D_C$  can be determined in the same way as  $K_B$  and  $D_B$  by measuring the nonlinear force deflection diagrams of the tabs and using equation (2) to calculate

$$K_{CV} = C_{ev}^i(\gamma) \gamma_{va}^2 \quad D_{CV} = C_{va}^{\prime\prime}(\gamma) \gamma_{va}^2 \quad (21)$$

The term  $\gamma_{va}$  denotes the tab rotation in the line where the force acting on the tab is applied. The matrix  $M_C$  can be determined by test or calculation. The elements of the coupling matrix

$$M_{AC} = M_{CA}^T = \phi_A^T A \phi_C \quad (22)$$

can be found by integration over the tab surface  $S_{CV}$

$$M_{AC,rv} = \int_{S_{CV}} \{ f_v m_{tv} h_r \gamma_v + [I_{tv} + f_v m_{tv} (b_v + f_v)] \alpha_r \gamma_v \} dl_t \quad (23)$$

where the following terms correspond to the  $v$ th tab (part of the  $v$ th control)

- $m_{tv}$  mass of the tab per unit span
- $I_{tv}$  mass moment of inertia per unit span referred to the center of gravity
- $f_v$  distance between the tab hinge axis and the tab center of gravity (see fig. 7)
- $b_v$  distance between the tab hinge axis and the control hinge axis (see fig. 7)

The quantities  $I_{tv}$ ,  $m_{tv}$ ,  $f_v$ , and  $b_v$  as well as  $h_r$ ,  $\alpha_r$ , and  $\gamma_v$  (see fig. 7) are functions of the tab span coordinate  $l_t$ . The elements of the coupling matrix

$$M_{BC} = M_{CB}^T = \phi_B^T A \phi_C \quad (24)$$

between the control surfaces and the appertaining tabs can be calculated by integration over the tab surface  $S_{CV}$

$$M_{BC,vv} = \int_{S_{CV}} [I_{tv} + m_t f_v (b_v + f_v)] \beta_v \gamma_v dl_t \quad (25)$$

Provided that the normal modes  $\phi_{Ar}$  can be measured with ideally locked control and tab hinges, neither hinge damping forces nor hinge stiffness forces are generated in  $\phi_{Ar}$ . This leads to

$$\left. \begin{aligned} K_{AC} = K_{CA}^T &\equiv 0 & K_{BC} = K_{CB}^T &\equiv 0 \\ D_{AC} = D_{CA}^T &\equiv 0 & D_{BC} = D_{CB}^T &\equiv 0 \end{aligned} \right\} \quad (26)$$

### Concept II

As described in references 1, 6, and 7, the replacement of the control nonlinearities by artificial linear stiffnesses results in a modified linearized test configuration represented in matrix notation by

$$A_L \ddot{u} + B_L \dot{u} + C_L u = P \quad (27)$$

which is formulated in terms of physical displacements. The governing dynamic equations of the unchanged nonlinear system can be written in the same form as equation (4) by subdividing the matrices A, B, and C as follows:

$$\left. \begin{aligned} A &= A_L - \Delta A_L + \Delta A_{NL} \\ B &= B_L - \Delta B_L + \Delta B_{NL} \\ C &= C_L - \Delta C_L + \Delta C_{NL} \end{aligned} \right\} \quad (28)$$

The term  $\Delta A_{NL} - \Delta A_L$  represents the difference in the mass distribution between the artificial linear system and the real nonlinear system;  $\Delta B_L$  and  $\Delta C_L$  define the damping and stiffness properties of the artificial linear elements;  $\Delta B_{NL}$  and  $\Delta C_{NL}$  describe the damping and stiffness properties of the replaced nonlinear elements. Development of the arbitrary displacement vector  $u$  in a series expansion of the measured normal modes  $\phi_{Lr}$  of the linearized system yields

$$u = \phi_L q \quad (29)$$

Inserting this modal transformation into equation (4), premultiplying by  $\phi_L^T$ , and taking into account equation (28) results in generalized equations of motion in the same form as equation (12), but with the mass, damping, and stiffness matrices now defined as

$$\left. \begin{aligned} M &= M_L - \Delta M_L + \Delta M_{NL} \\ D &= D_L - \Delta D_L + \Delta D_{NL} \\ K &= K_L - \Delta K_L + \Delta K_{NL} \end{aligned} \right\} \quad (30)$$

The matrices  $M_L$ ,  $D_L$ , and  $K_L$  are measured in a GVT on the linearized system. Furthermore,

$$\left. \begin{aligned} \Delta M_{NL} - \Delta M_L &= \phi_L^T (\Delta A_{NL} - \Delta A_L) \phi_L \\ \Delta D_{NL} - \Delta D_L &= \phi_L^T (\Delta B_{NL} - \Delta B_L) \phi_L \\ \Delta K_{NL} - \Delta K_L &= \phi_L^T (\Delta C_{NL} - \Delta C_L) \phi_L \end{aligned} \right\} \quad (31)$$

For simplicity, consider only one control surface. For the  $v$ th control surface, the modal matrix  $\phi_L$  degenerates to the row matrix

$$\phi_{vL} = [\beta_{v1}, \beta_{v2}, \dots, \beta_{vr}, \dots, \beta_{vn}] \quad (32)$$

and  $\Delta B_{NL} - \Delta B_L$  and  $\Delta C_{NL} - \Delta C_L$  degenerate to the  $1 \times 1$  matrices

$$\left. \begin{aligned} \Delta B_{NL} - \Delta B_L &= \frac{C_e''(\beta)}{\omega} - B_L \\ \Delta C_{NL} - \Delta C_L &= C_e'(\beta) - C_L \end{aligned} \right\} \quad (33)$$

where the nonlinear stiffness and damping values  $C_e'(\beta)$  and  $C_e''(\beta)$  can be determined again by applying equation (2) to the measured nonlinear force deflection diagram. The damping and stiffness matrices  $B_L$  and  $C_L$ , respectively, of the artificial linear element can be measured by means of simple tests. The matrix  $\Delta M_{NL} - \Delta M_L$  can also be calculated by using the modal matrix as defined in equation (32), provided the two parts of the  $1 \times 1$  matrix  $\Delta A_{NL} - \Delta A_L$  can be defined as moments of inertia by referring the removed mass of the nonlinear system, as well as the additional mass resulting from the artificial linearization, to the hinge angle  $\beta$ .

### Concept III

The aeroelastic equations of an airplane can also be established by means of both a set of normal modes measured in a GVT with controls removed and rigid-body and some elastic normal modes of the several controls (see fig. 10) determined experimentally or by fairly simple calculations. The equations of motion of the coupled system can be set up by means of Lagrange's equations

$$\frac{\partial}{\partial T} \left( \frac{\partial T}{\partial \dot{q}_r} \right) + \frac{\partial U}{\partial q_r} + \frac{\partial W}{\partial \dot{q}_r} = \sum_{\ell=1}^{\sigma} \lambda_{\ell} \frac{\partial g_{\ell}}{\partial q_r} \quad (34)$$

$$(r = 1, 2, \dots, n_A, n_A + 1, \dots, n_B, \dots, n_i, \dots)$$

where

$$\left. \begin{aligned} 2T &= M\dot{q}^2 \\ 2U &= Kq^2 + \Delta K q^2 \\ 2W &= D\dot{q}^2 + \Delta D \dot{q}^2 \end{aligned} \right\} \quad (35)$$

The matrices  $\Delta K$  and  $\Delta D$  in equation (35) take into account the elastic coupling between control surfaces and main structure by means of the real hinge stiffness and hinge damping elements. The term on the right side of equation (34) is formulated in terms of Lagrange's undetermined multipliers  $\lambda_{\ell}$  which correspond to a number of  $\sigma$  constraint conditions

$$g_{\ell}(q_1, q_2, \dots, q_r, \dots, q_{n_i}) = 0 \quad (\ell = 1, 2, \dots, \sigma) \quad (36)$$

They express compatibility in those coupling points, where the controls can be assumed to be rigidly fixed to the main structure. Application of equation (34) to equations (35) and (36) yields

$$M\ddot{q} + (D + \Delta D)\dot{q} + (K + \Delta K)q - \psi^T \lambda = 0 \quad (37)$$

where the elements of the  $r \times \ell$  matrix  $\psi^T$  are

$$\Psi_{qr}^T = \frac{\partial g}{\partial q_r} \quad (38)$$

Confining the further derivation to the coupling of only two systems, A and B (main structure and control surface) results in the following generalized mass, stiffness, and damping matrices of the uncoupled system:

$$\left. \begin{aligned} M &= \begin{bmatrix} M_A & 0 \\ 0 & M_B \end{bmatrix} & D &= \begin{bmatrix} D_A & 0 \\ 0 & D_B \end{bmatrix} \\ K &= \begin{bmatrix} K_A & 0 \\ 0 & K_B \end{bmatrix} \end{aligned} \right\} \quad (39a)$$

where the submatrices are

$$M_i = \phi_i^T A_i \phi_i \quad K_i = \phi_i^T C_i \phi_i \quad D_i = \phi_i^T B_i \phi_i \quad (i = A, B) \quad (39b)$$

The matrices  $A_i$ ,  $B_i$ , and  $C_i$  describe mass, damping, and stiffness of the subsystems A and B in terms of geometrical coordinates;  $\phi_i$  is the modal matrix of subsystem  $i$ . The elements of the diagonal matrices  $M_i$  and  $K_i$  and of the damping matrices  $D_i$ , which are not necessarily diagonal, can be determined by GVT or, as in the case of the controls, by calculation, also.

According to reference 7 the generalized coupling matrices  $\Delta K$  and  $\Delta D$  can be written as follows:

$$\Delta K = \phi_{AB}^T C_{AB} \phi_{AB} \quad \Delta D = \phi_{AB}^T B_{AB} \phi_{AB} \quad (40)$$

When the main structure and control surface are coupled by one single complex hinge stiffness  $C_e$  in the action line of the control force, we obtain

$$\phi_{AB} = \left[ \begin{array}{c|cccc} \text{A} & \text{A} & & \text{A} & \\ \alpha_{a1} & \alpha_{a2} & \dots & \alpha_{an} & \\ \hline & & 0 & & \\ \hline & & & & \text{B} \\ & & & & \alpha_{a,n+1} & \alpha_{a,n+2} & \dots & \alpha_{anB} \end{array} \right] \quad (41)$$

$$C_{AB} = C_e' \begin{bmatrix} 1 & -1 \\ -1 & 1 \end{bmatrix} \quad B_{AB} = \frac{C_e''}{\omega} \begin{bmatrix} 1 & -1 \\ -1 & 1 \end{bmatrix} \quad (42)$$

The angles of rotation  $\alpha_{ar}^A$  and  $\alpha_{ar}^B$  are defined in figure 9. For the special case of coupling two systems A and B the compatibility condition for  $\sigma$  physical degrees of freedom can be expressed by the constraints

$$g_l = u_l^A - u_l^B = 0 \quad (l = 1, 2, \dots, \sigma) \quad (43)$$

If  $u_l^A$  and  $u_l^B$  are expressed in a series of the normal modes of the systems A and B, then

$$g_l = \sum_{r=1}^{n_A} u_{lr}^A q_r - \sum_{r=n_A+1}^{n_B} u_{lr}^B q_r = 0 \quad (44)$$

or in matrix notation

$$g = \Psi q = 0 \quad (45)$$

The aeroelastic equations of motion are defined now by the  $n_A + n_B = m$  generalized coordinates. Due to the  $\sigma$  constraints there remains a number of  $c = m - \sigma$  independent generalized coordinates in terms of which the aeroelastic equations have to be formulated. To do this, the term  $\Psi^T$  in equation (37) has to be rearranged rowwise so that

$$\Psi^T \rightarrow \bar{\Psi}^T = \begin{bmatrix} \Psi_\epsilon \\ \Psi_\sigma \end{bmatrix} \quad (46)$$

where  $\Psi_\sigma$  is a nonsingular  $\sigma \times \sigma$  matrix. The matrices M, K, D,  $\Delta K$ , and  $\Delta D$  with respect to both their columns and rows and the column matrix q have to be rearranged in the same sense. The rearranged equations can be written as

$$\bar{M}\ddot{\bar{q}} + (\bar{D} + \Delta\bar{D})\dot{\bar{q}} + (\bar{K} + \Phi\bar{K})\bar{q} = \bar{\Psi}^T \lambda \quad (47)$$

where

$$\bar{q} = [p^T, q_\sigma^T]^T \quad (48)$$

The new structure of the matrices  $\bar{M}$ ,  $\bar{D}$ ,  $\bar{K}$ ,  $\Delta\bar{D}$ , and  $\Delta\bar{K}$  is shown in the following equation using  $\bar{M}$  as an example

$$\bar{M} = \begin{bmatrix} M_{\epsilon\epsilon} & M_{\epsilon\sigma} \\ M_{\sigma\epsilon} & M_{\sigma\sigma} \end{bmatrix} \quad (49)$$

Thus,  $\lambda$  can be determined as follows

$$\lambda = (\bar{\Psi}^T)^{-1} \left\{ [M_{\sigma\epsilon}, M_{\sigma\sigma}] \ddot{\bar{q}} + ([D_{\sigma\epsilon}, D_{\sigma\sigma}] + [\Delta D_{\sigma\epsilon}, \Delta D_{\sigma\sigma}]) \dot{\bar{q}} + ([K_{\sigma\epsilon}, K_{\sigma\sigma}] + [\Delta K_{\sigma\epsilon}, \Delta K_{\sigma\sigma}]) \bar{q} \right\} \quad (50)$$

From equations (45) and (46) it follows that

$$q_\sigma = -\Psi_\sigma^{-1} \Psi_\epsilon p \quad (51)$$

Inserting equation (50) into the first  $\epsilon$  rows of equation (47) and taking into account equation (51) results in the following equation

$$\begin{aligned} & (M_{\epsilon\epsilon} - M_{\epsilon\sigma} X - X^T M_{\sigma\epsilon} + X^T M_{\sigma\sigma} X) \ddot{p} \\ & + \left\{ D_{\epsilon\epsilon} + \Delta D_{\epsilon\epsilon} - (D_{\epsilon\sigma} + \Delta D_{\epsilon\sigma}) X - X^T (D_{\sigma\epsilon} + \Delta D_{\sigma\epsilon}) + X^T (D_{\sigma\sigma} + \Delta D_{\sigma\sigma}) X \right\} \dot{p} \\ & + \left\{ K_{\epsilon\epsilon} + \Delta K_{\epsilon\epsilon} - (K_{\epsilon\sigma} + \Delta K_{\epsilon\sigma}) X - X^T (K_{\sigma\epsilon} + \Delta K_{\sigma\epsilon}) + X^T (K_{\sigma\sigma} + \Delta K_{\sigma\sigma}) X \right\} p = 0 \end{aligned} \quad (52)$$

where

$$X = \Psi_\sigma^{-1} \Psi_\epsilon \quad (53)$$

It can easily be shown that equation (52) can be transformed to the more convenient equation

$$y^T \bar{M} \ddot{y} + y^T (\bar{D} + \Delta \bar{D}) \dot{y} + y^T (\bar{K} + \Delta \bar{K}) y = 0 \quad (54)$$

$$\text{where } y = \begin{bmatrix} I \\ -X \end{bmatrix} \quad (55)$$

with the unity matrix  $I$ . It should be mentioned that a nonsingular matrix  $\Psi_0$  can be determined optimally by applying common mathematical tools for the determination of the linear independence of a given number of vectors, as described, for example, in reference 8. These methods are also applicable to cases with the number of constraints higher than the rank of matrix  $\Psi_0$ . Practical applications to structural dynamics problems are presented in reference 9.

It is obvious that the unsteady aerodynamic forces cannot immediately be calculated on the basis of the separate normal mode sets of the several substructures (main structure and control surfaces). However, this problem can easily be solved as follows:

(1) Couple the controls to the main structure using the above described procedure. In doing so, the actual nonlinear stiffnesses  $C_e$  are replaced by linear stiffnesses chosen to be an average representative of the nonlinear ones.

(2) Calculate the normal mode characteristics of this linearly coupled system and calculate the unsteady aerodynamic forces based on this set of normal modes.

(3) In the case of hinge stiffness variations or nonlinear flutter calculations, the combination of concepts III and II described subsequently may be used.

#### Combined Application of Concepts I, II, and III

A detailed examination of the possibilities offered by the three concepts makes it obvious that sometimes their combined application may be very beneficial. Four possible variations can be outlined as follows:

##### Combination of Concept III and Concept II:

(1) Apply Concept III, taking into account linear and lightly damped hinge coupling elements.

(2) Calculate the normal mode characteristics of the linearly coupled system.

(3) Vary the linear coupling elements or introduce the nonlinear coupling elements by means of Concept II.

Combination of Concept III and Concept I:

(1) Apply Concept III with a completely rigid coupling including the control hinge degrees of freedom resulting in a configuration with rigidly locked controls.

(2) Take into account the control degrees of freedom according to Concept I by adding a separate set of control normal modes with the main structure at rest.

Combination of Concept II and Concept I:

(1) Test the aircraft structure with controls removed as a basic configuration.

(2) Establish analytically a second configuration with the controls rigidly locked to the main structure by applying Concept II. This can be achieved by adding modal mass coupling matrices  $\Delta M$  to the equations of motion of the basic configuration similar to those defined in equation (31).

When a single control surface is considered the coefficients of the mass coupling matrix  $\Delta M$  can be written as

$$\Delta M_{rs} = \phi_{Rr}^T \Delta A_R \phi_{Rs} \quad (56)$$

where

$$\phi_{Rr}^T = [u_{xr}, u_{yr}, u_{zr}, \eta_{xr}, \eta_{yr}, \eta_{zr}] \quad (57)$$

The column matrix  $\phi_{Rr}$  represents the translational and rotational displacements at the coupling point of the main structure in relation to the XYZ axis system (see fig. 10). If the center of gravity of the control lies outside the coupling point,  $(x_s, y_s, z_s) = (s_x, 0, s_z)$ , the inertia matrix  $\Delta A_R$  can be written in the form

$$\Delta A_R = \begin{bmatrix} m_R & & & 0 & & & m_R s_z & & 0 \\ & m_R & & -m_R s_z & & & 0 & & m_R s_x \\ & & m_R & 0 & & & -m_R s_x & & 0 \\ 0 & -m_R s_z & 0 & I_{Rx} + m_R s_z^2 & & & 0 & & -m_R s_z s_x \\ m_R s_z & 0 & -m_R s_x & 0 & & I_{Ry} + m_R (s_z^2 + s_x^2) & & & 0 \\ 0 & m_R s_x & 0 & -m_R s_x s_z & & 0 & & & I_{Rz} + m_R s_x^2 \end{bmatrix} \quad (58)$$

where

$m_R$  mass of the control surface  
 $I_{Rx}, I_{Ry}, I_{Rz}$  mass moments of inertia of the control surface in  
relation to its center of gravity

(3) Take into account the control degrees of freedom according to Concept I by adding a separate set of control normal modes with the main structure at rest.

Combination of Concept II and Concept III:

(1) Test the aircraft structure with rigid control dummies in locked condition as a basic configuration. The rigid dummies are used to determine a better basic set of normal mode shapes representing the dynamic deformations of the coupled system than can be determined in the test configuration with removed controls. This procedure can best be described as convergence acceleration by means of interface loading.

(2) Establish analytically a second configuration with the dummy controls removed. This can be achieved in accordance with Concept II by subtracting a modal mass coupling matrix  $\Delta M$  as defined in equation (56) from the equations of motion of the basic configuration.

(3) Apply Concept III coupling the elastic controls to the main structure.

COMPARATIVE CONSIDERATIONS

The concepts presented offer a number of possibilities to incorporate the control systems of light airplanes, which in general are affected by strong concentrated nonlinearities, into the flutter analysis. Special emphasis is placed on the mathematical modeling of the elastomechanical system based on GVT. It is obvious that a final evaluation of the applicability and accuracy of the different concepts is rather difficult because, up to the present time, only Concept I has been applied to some extent to real airplane structures. Only little experience with the other concepts is at hand. Thus, Concept II has recently been employed in the course of the flutter clearance process of the soaring airplane ASW-15. Flutter calculations based on this concept predicted tail flutter at about 200 km/hr. That result was verified by flight flutter tests, where the airplane showed nonlinear flutter in a speed range from 175 to 220 km/hr, starting with comparably small amplitudes at 175 km/hr and increasing to very high amplitudes far beyond the regular rudder stroke at higher speeds. This behavior in concurrence with substantial alterations of the flutter modes is symptomatic of highly nonlinear flutter cases. A more detailed consideration of this special problem exceeds the subject of this paper and should be reserved for further investigations.

It is also worth mentioning that the ground vibration test carried out in accordance with this concept took far less test time than a normal test on the unchanged structure (reduction of about 80%).

The first comparative investigation of the Concepts I, II, and III has been the special concern of reference 10, where results are reported for a simple plate-type wing-aileron model with largely linear elastodynamical properties. Although this model cannot be considered representative in all respects of the elastodynamical behavior of real airplanes, it seems to be opportune to use the results of this investigation together with the present experience with the Concepts I and II as a basis for a preliminary assessment concerning the advantages and the weak points of different methods. For this purpose a selected number of criteria is used taking into consideration several requirements such as

- (1) Test effort required
- (2) Numerical effort required
- (3) General applicability
- (4) Physical consistency

Table 1 shows in a condensed form how the criteria are met by the several concepts.

#### CONCLUDING REMARKS

It has been known for many years that the flutter clearance of light airplanes can be highly afflicted by uncertainties stemming from strong localized nonlinearities in the control mechanisms. It is shown that the establishment of more reliable and accurate mathematical models for the flutter analysis requires modified ground vibration test procedures combined with suitably adapted modal synthesis approaches. Three basic concepts with several variations have been described in detail. They offer a diverse choice of tools for carrying out both approximately linearized and nonlinear flutter investigations.

A comparative consideration has been made as to the capacity as well as the drawbacks of the different concepts. However, because of lack of practical experience with Concepts II and III, it is not possible at present to make a conclusive evaluation.

#### REFERENCES

1. Breitbach, E.: Effects of Structural Non-Linearities on Aircraft Vibration and Flutter. AGARD Report No. 665, Sept. 1977.
2. Dat, R.; Trétout, R.; and Lafont, J. M.: Essais de Vibration d'une Structure Comportant du Frottement Sec. La Rech. Aérospatiale, No. 3, 1975, pp. 169-174.
3. Bogoljubow, N. N.; and Mitropolski, J. A.: Asymptotische Methoden in der Theorie der nichtlinearen Schwingungen. Akademie-Verlag, Berlin, 1965.
4. Scanlan, R. H.; and Rosenbaum, R.: Introduction to the Study of Aircraft Vibration and Flutter. MacMillan Co., 1951.
5. Küssner, H. G.; and Göllnitz, H.: Theorie und Methode der Flatterrechnung von Flugzeugen unter Benutzung des Standschwingungsversuchs. AVA-Forschungsbericht 64-01, 1964.
6. Küssner, H. G.; and Breitbach, E.: Bestimmung der Korrekturglieder der Bewegungsgleichungen bei Änderungen eines elastomachanischen Systems. AVA-Report 69 J 01, 1969.
7. Breitbach, E.: Investigation of Spacecraft Vibrations by Means of the Modal Synthesis Approach. ESA-SP-121, Oct. 1976, pp. 1-7.
8. Courant, R.; and Hilbert, I.: Methoden der mathematischen Physik I. Heidelberg Taschenbücher, Springer-Verlag, 1968.
9. Walton, W. C.; and Steeves, E. C.: A New Matrix Theorem and Its Application for Establishing Independent Coordinates for Complex Dynamical Systems With Constraints. NASA TR R-326, 1969.
10. Hüners, H.: Berücksichtigung der Ruderfreiheitsgrade im Flatternachweis von Flugzeugen. DFVLR-Report IB 253-78 J 07, 1978.

TABLE 1.- COMPARATIVE CONSIDERATION OF CONCEPTS I, II, AND III

Criterion	Concept I	Concept II	Concept III
Test effort	Low - locking the several controls and tabs	Medium - replacement of the real hinge stiff-nesses by linear ones	Medium - removal of the controls
Preparation time	Very low - no angle measurements	Low - angle measurement in the hinge stiffness points	Low/medium - angle measure-ment in coupling points, several substructures
Test equipment	Low - regular number of accelerometers, no angle measurements	Medium - more accel-erometers in the hinge stiffness points	Medium/high - high number of accelerometers at cou-pling points, several substructures
Measuring accuracy	Regular accuracy sufficient	Higher accuracy required - angle measurement	Higher accuracy required - angle measurement
Numerical effort	Low/medium - integration over mass distribution of controls	Low - very simple deter-mination of coupling matrices	Medium - calculation of normal modes of coupled system necessary
Physical consistency and general application	Low - most normal modes without hinge angle	Low/medium - all normal modes affected with hinge angles	Low/medium - all normal modes affected with hinge angles
Convergence	Good - for controls without resonances in the frequency range of interest	Excellent - statically indeterminate coupling included	Good - can be improved by interface loading, stat-ically indeterminate coupling included
Type of controls	Restricted to controls without resonances in the frequency range of interest, small size	No restrictions - con-trols can be very flexible and large	No restrictions - controls can be very flexible and large
Nonlinearities	No restrictions - low number of nonlinear coupling terms	No restrictions, but higher number of non-linear coupling terms	No restrictions, but higher number of nonlinear cou-pling terms

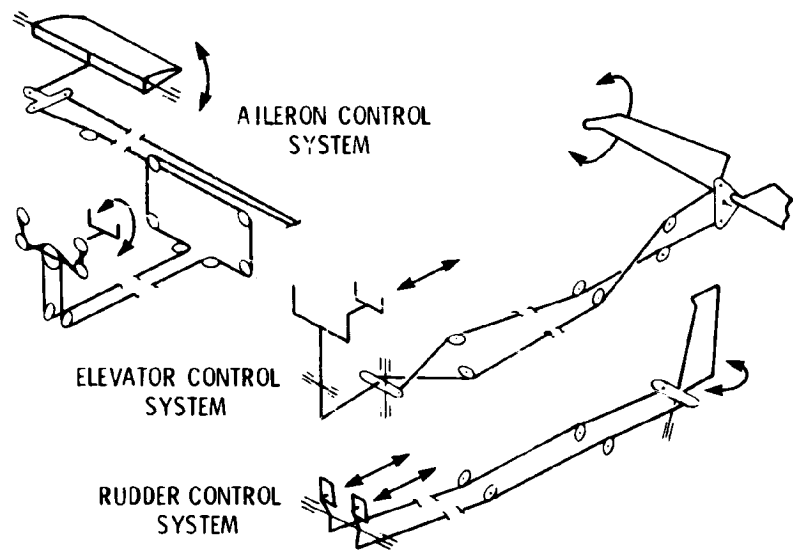
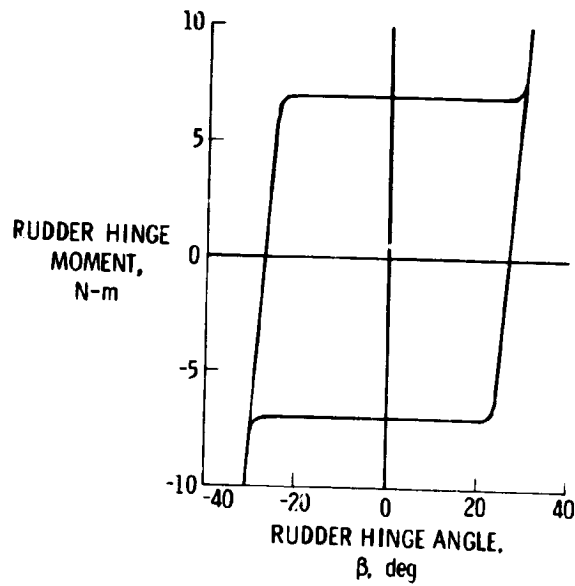
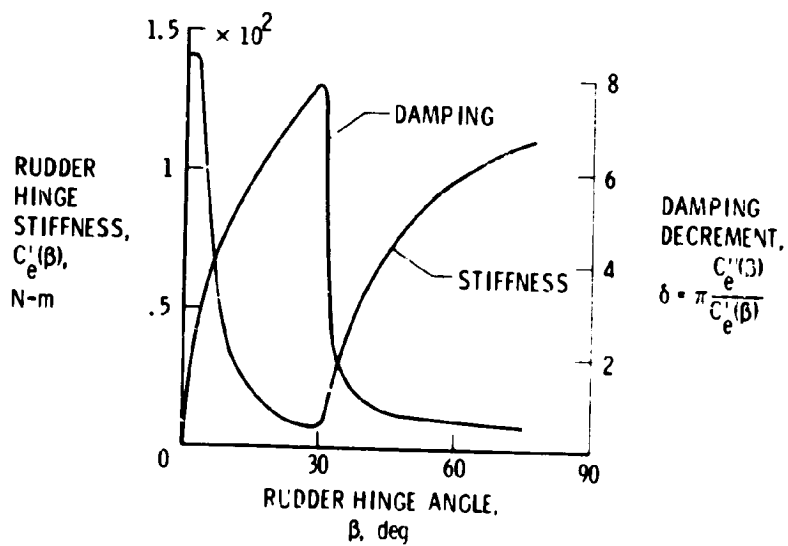


Figure 1.- Schematical sketch of the control system of a light airplane.

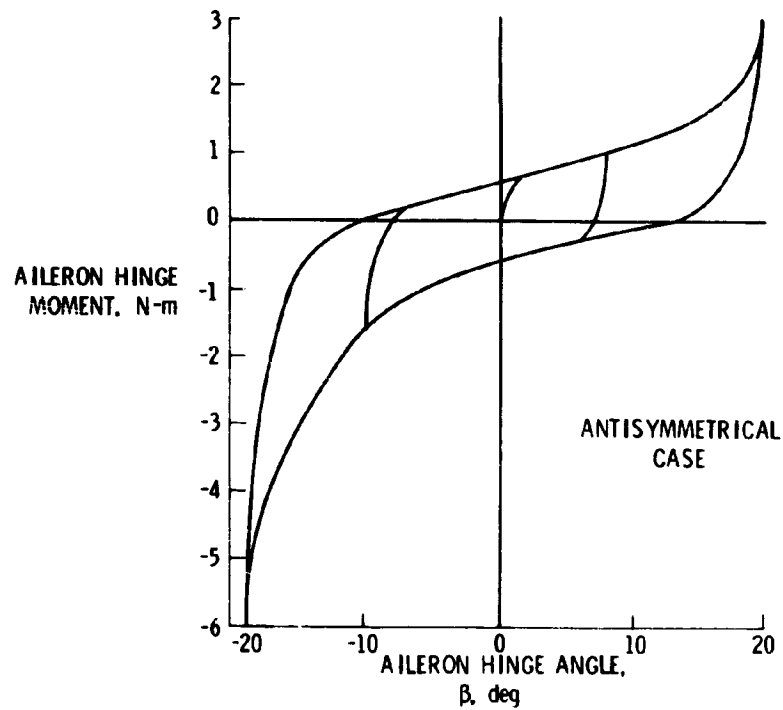


(a) Force deflection diagram.

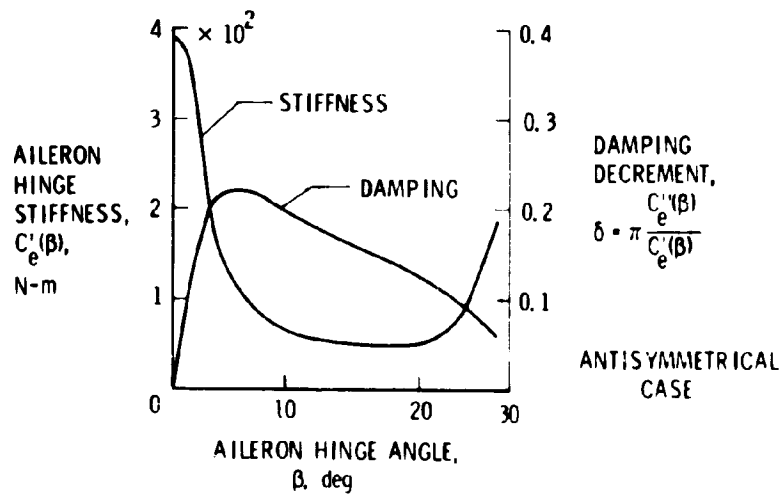


(b) Hinge stiffness and damping versus hinge angle.

Figure 2.- Force deflection diagram and stiffness and damping for the rudder system of a soaring airplane.

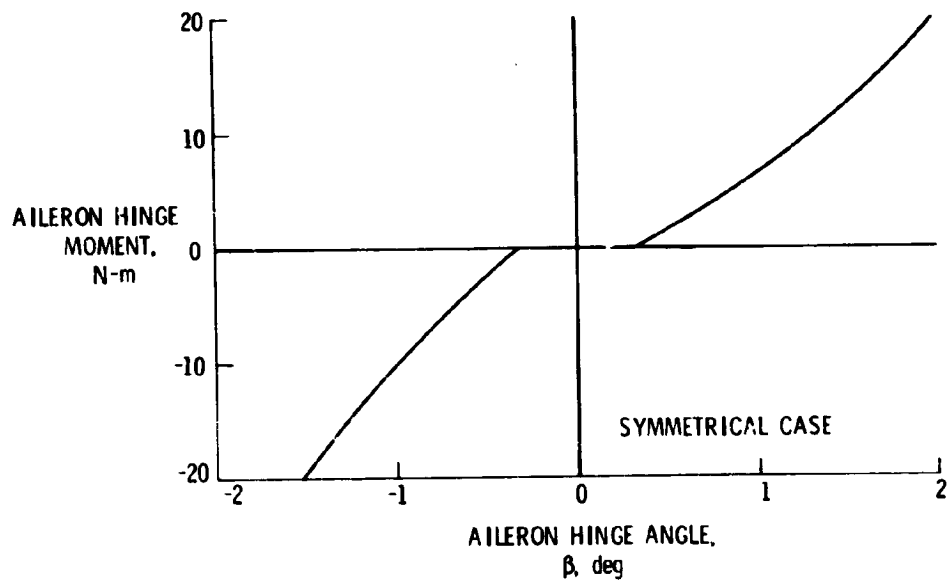


(a) Force deflection diagram.

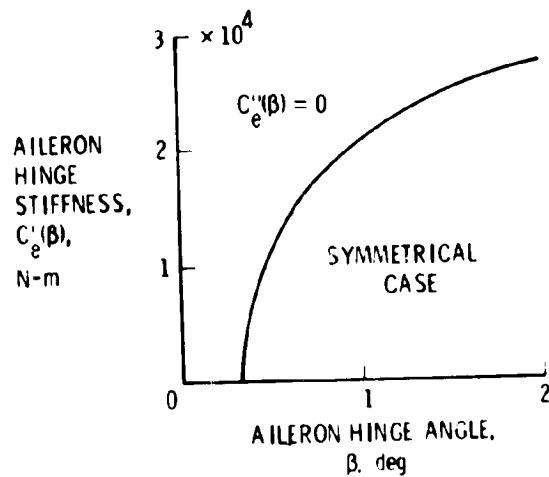


(b) Hinge stiffness and damping versus hinge angle.

Figure 3.- Force deflection diagram and stiffness and damping for the aileron system of a soaring airplane. Antisymmetrical case.



(a) Force deflection diagram.



(b) Hinge stiffness and damping versus hinge angle.

Figure 4.- Force deflection diagram and stiffness and damping for the aileron system of a soaring airplane. Symmetrical case.

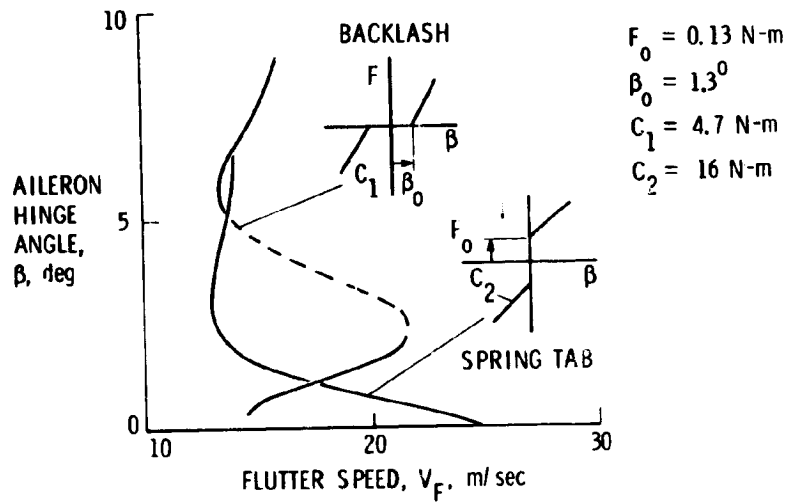


Figure 5.- Measured flutter boundary of a nonlinear model.

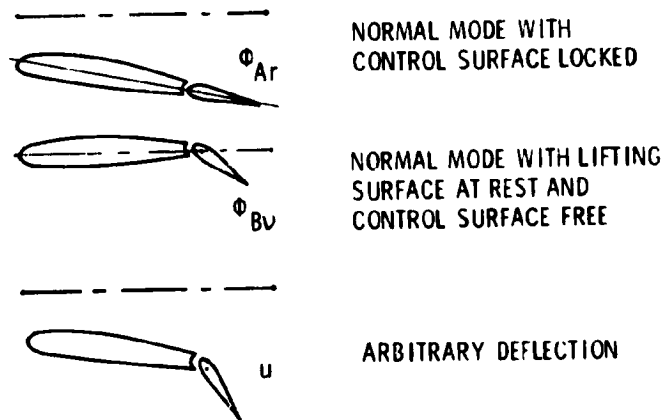


Figure 6.- Modal superposition according to concept I. Controls without tabs.

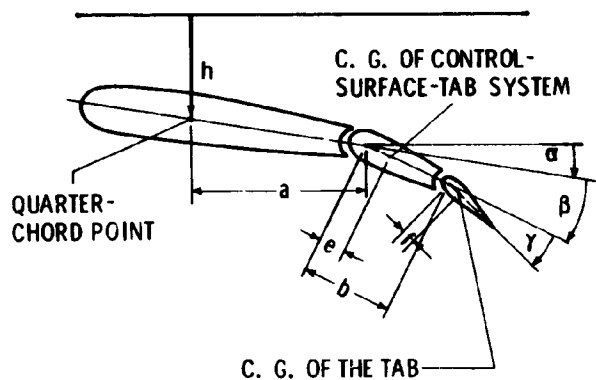


Figure 7.- Lifting surface with control surface and tab.

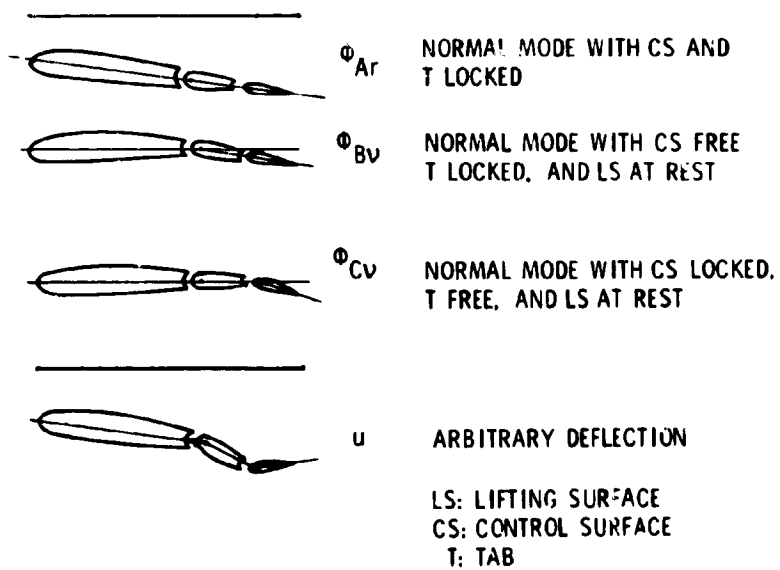


Figure 8.- Modal superposition according to concept I. Controls with tabs.

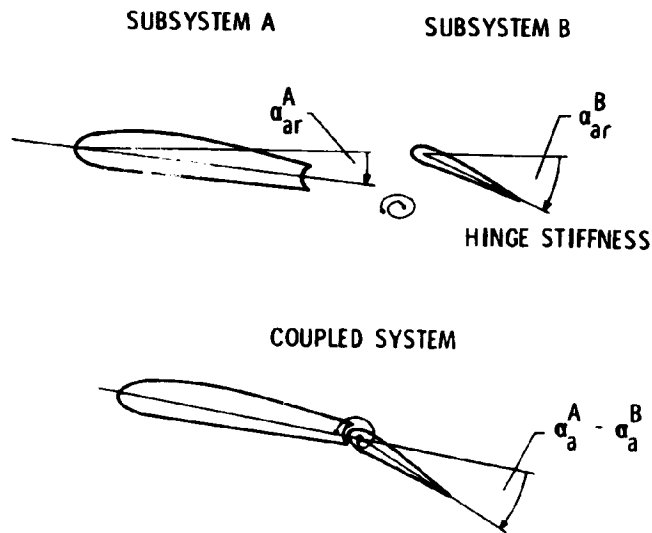
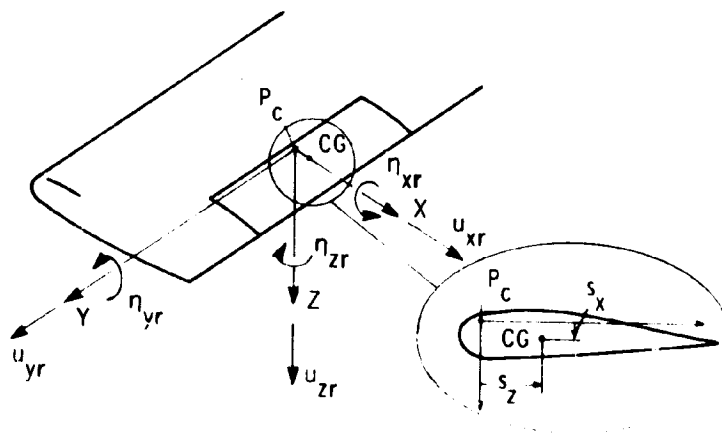


Figure 9.- Modal coupling of a wing control surface system according to concept III.



$P_c$  COUPLING POINT  
 $CG$  CENTER OF GRAVITY

Figure 10.- Modal coupling according to a combination of concepts I and II.

N79-27079<sup>29</sup>

## ADVANCED COMPOSITES IN SAILPLANE STRUCTURES:

### APPLICATION AND MECHANICAL PROPERTIES

Dieter Muser

Research Center Stuttgart  
Deutsche Forschungs- und Versuchsanstalt  
für Luft- und Raumfahrt e.V.

### SUMMARY

Advanced Composites in Sailplanes mean the use of carbon and aramid fibers in an epoxy matrix. Weight savings are in the range of 8 to 18% in comparison with glass fiber structures. The laminates will be produced by hand-layup techniques and all material tests shown here have been done with these materials. These values may be used for calculation of strength and stiffness as well as for comparison of the materials to get a weight-optimum construction. Proposals for material-optimum construction are mentioned.

### TECHNICAL HISTORY

The first fiber-reinforced glider, a Phoenix developed by Prof. Eppler, made its maiden flight in 1957. Now, more than 4000 gliders with glass-fiber-reinforced structures are in the air all over the world. Increasing the wing loading permitted increases in maximum speed, but structural demands increased the weight also.

A large span enabled the constructors to build planes with lift to drag ratios of about 50 (ASW 17: 48.5, Nimbus 2: 49) and sinking speeds of 0.50 m/s (1.64 ft/s). But it was not possible to realize wing spans with more than 22 meters without a very soft wing structure. This was possible when carbon fibers were used in the center wing section of the Akaflieg Braunschweig SB 10 in 1972 (fig. 1). With a maximum wing span of 29 meters, this glider has the best glide ratio of 53 and a sinking speed of 0.41 m/s (1.35 ft/s). But the price of carbon fibers was very high at this time and so this material was used only in another prototype, the Akaflieg Stuttgart fs-29 in 1975. To realize the old dream to vary the span during flight, it was absolutely necessary to use carbon fibers in the outer moving part of the wing and in the spar of the inner wing section. When the Akaflieg Braunschweig built the first all-carbon glider in 1977/78, they used carbon fibers to reduce weight and to stiffen the wing, so that all flaps move only very slightly and the pilot is able to handle them. And this was the year when carbon fibers were used in a larger volume in different types of commercial gliders.